

# [CI] を用いた高赤方偏移銀河での分子ガス探査

## 参考文献

Offner et al. 2014, MNRAS, 440 L81

Alaghband-Zadeh et al. 2013, MNRAS, 435, 1493

Ryu Makiya (IoA, JSPS fellow)

第二回 微細構造輝線研究会

# Motivation

- 宇宙の星形成史が知りたい
- そのために cold gas の進化が, 特に  $\text{H}_2$  の進化が知りたい
- 疑問
  - $\text{H}_2$  を真にトレースする観測量は何か?
  - 温度や密度分布は?
  - local との違いは?

# Atomic carbon : [C I]

- neutral ISM をトレース
- 炭素原子の微細構造輝線は  $^3P_2 \rightarrow ^3P_1$  と  $^3P_1 \rightarrow ^3P_0$  の二種類だけなので励起温度や質量などの物理量を決めやすい
- local galaxies を観測したところ, [C I] と CO は空間的にもよく相関している
  - [C I] を観測すれば CO の縮退も解ける
- [C I] は  $H_2$  のトレーサーとしても使える

# Fundamental parameters for C and CO

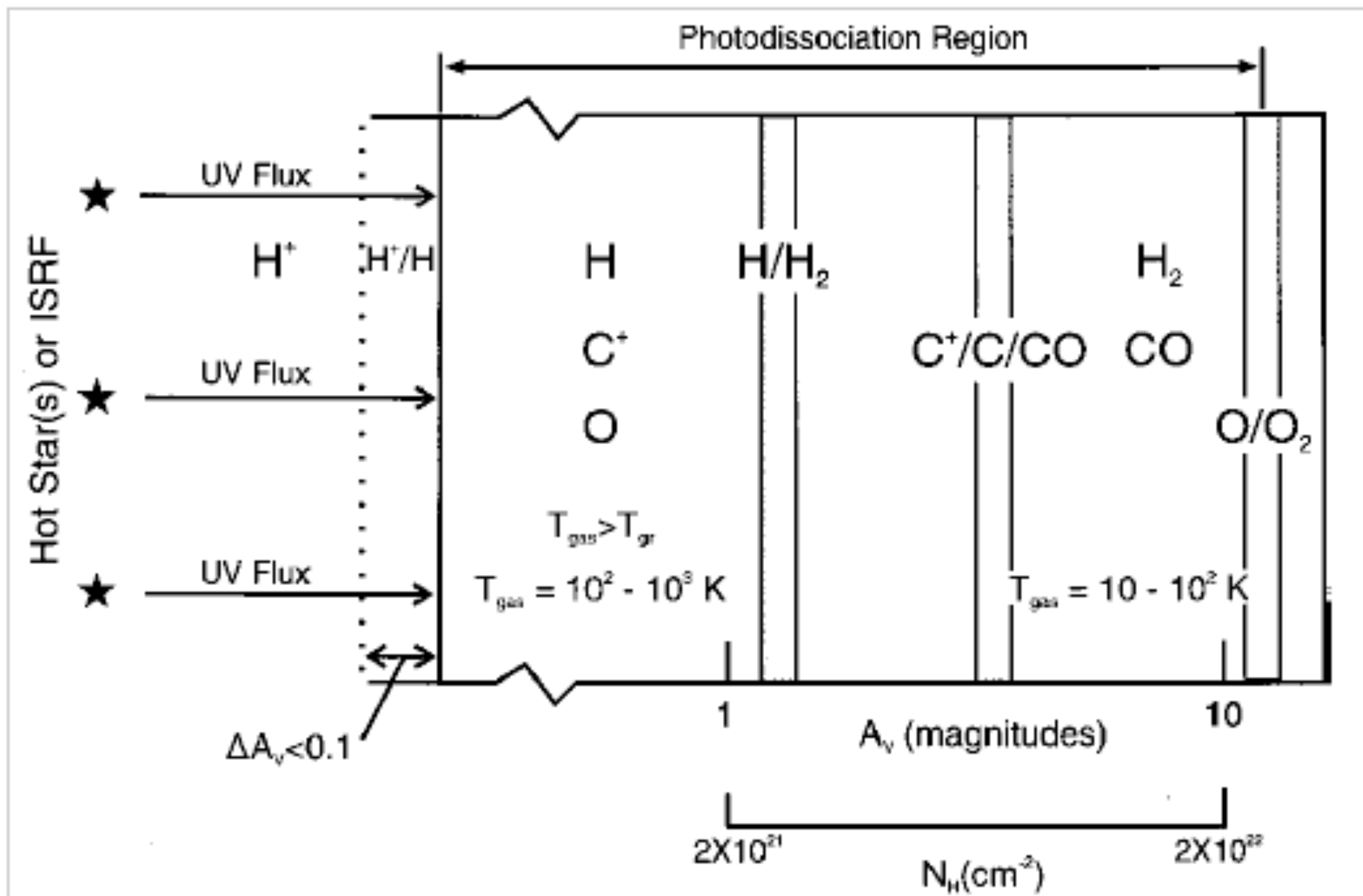
Table 1 Fundamental parameters for frequently observed molecules and fine structure lines

Species	Transition	Excitation potential (K)	$\lambda$ ( $\mu\text{m}$ )	$\nu$ (GHz)	Einstein A ( $\text{s}^{-1}$ )	$n_{\text{crit}}$ ( $\text{cm}^{-3}$ )
[C I]	$^3P_2 \rightarrow ^3P_1$	63	370.42	809.34	$2.7 \times 10^{-7}$	$1.2 \times 10^3$
	$^3P_1 \rightarrow ^3P_0$	24	609.14	492.16	$7.9 \times 10^{-8}$	470
CO	$J = 1-0$	5.5	2601	115.27	$7.2 \times 10^{-8}$	$2.1 \times 10^3$
	$J = 2-1$	16.6	1300	230.54	$6.9 \times 10^{-7}$	$1.1 \times 10^4$
	$J = 3-2$	33.2	867	345.80	$2.5 \times 10^{-6}$	$3.6 \times 10^4$
	$J = 4-3$	55.3	650.3	461.04	$6.1 \times 10^{-6}$	$8.7 \times 10^4$
	$J = 5-4$	83.0	520.2	576.27	$1.2 \times 10^{-5}$	$1.7 \times 10^5$
	$J = 6-5$	116.2	433.6	691.47	$2.1 \times 10^{-5}$	$2.9 \times 10^5$
	$J = 7-6$	154.9	371.7	806.65	$3.4 \times 10^{-5}$	$4.5 \times 10^5$
	$J = 8-7$	199.1	325.2	921.80	$5.1 \times 10^{-5}$	$6.4 \times 10^5$
	$J = 9-8$	248.9	289.1	1036.9	$7.3 \times 10^{-5}$	$8.7 \times 10^5$
	$J = 10-9$	304.2	260.2	1152.0	$1.0 \times 10^{-4}$	$1.1 \times 10^6$

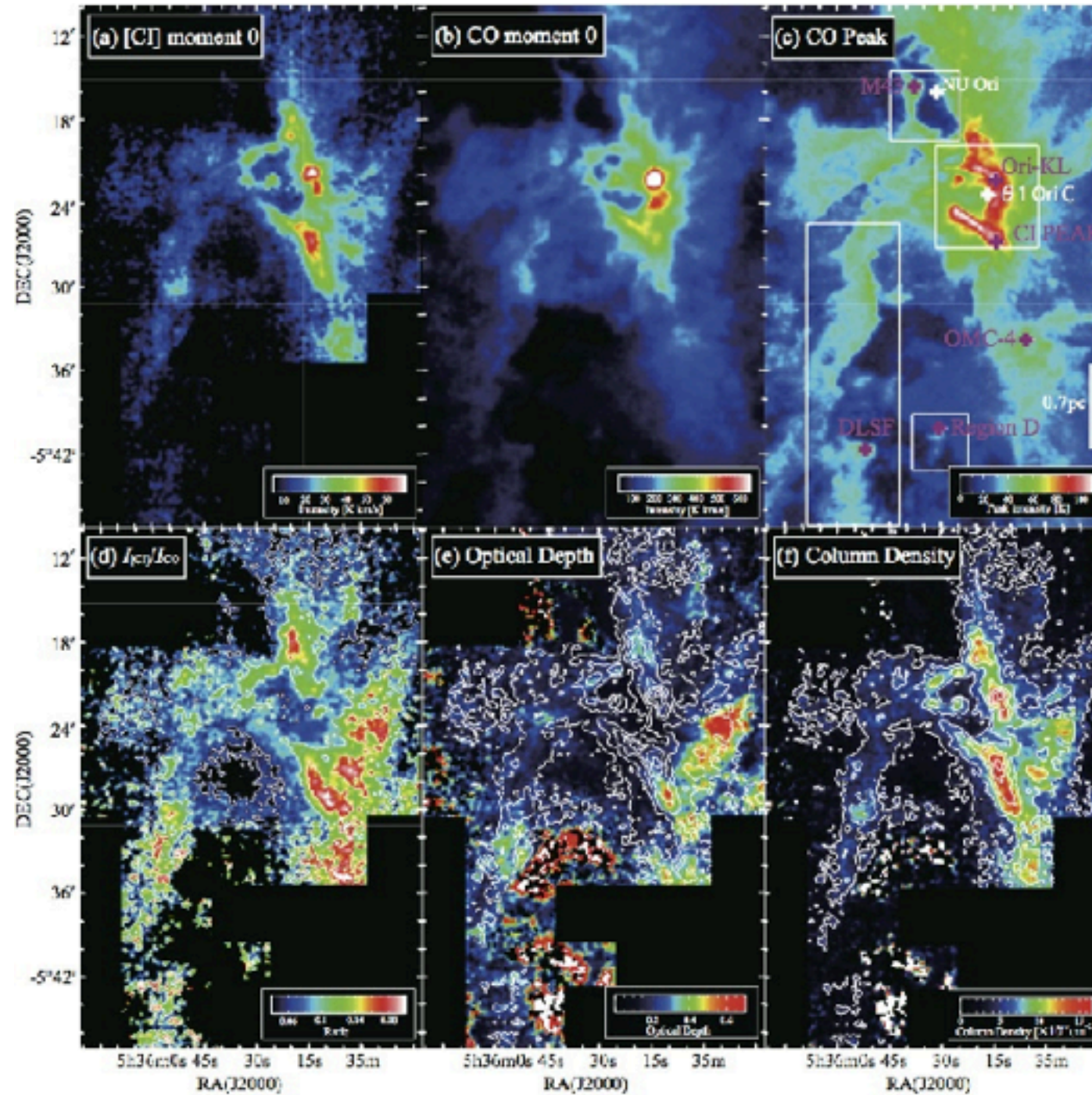
(ref: Carilli & Walter 2013)

- [C I] と CO の critical density は同程度
- 同じ領域から出ている？

# [C] はどこから？



# [CI] はどこから？



(ref:Shimajiri et al. 2013)

何となく (?) [CI] は PDR 起源だと思われていたが  
それでは実際の分布の説明がつかない

## An alternative accurate tracer of molecular clouds: the ‘ $X_{\text{CI}}$ -factor’

Stella S. R. Offner,<sup>1</sup> ★† Thomas G. Bisbas,<sup>2</sup> Tom A. Bell<sup>3</sup> and Serena Viti<sup>2</sup>

<sup>1</sup>*Department of Astronomy, Yale University, New Haven, CT 06511, USA*

<sup>2</sup>*Department of Physics and Astronomy, University College London, Gower Street, London WC1E 6B, UK*

<sup>3</sup>*Centro de Astrobiología (CSIC-INTA), Carretera de Ajalvir, km 4, E-28850 Madrid, Spain*

### ABSTRACT

We explore the utility of CI as an alternative high-fidelity gas-mass tracer for galactic molecular clouds. We evaluate the ‘ $X_{\text{CI}}$ -factor’ for the 609  $\mu\text{m}$  carbon line, the analogue of the CO ‘ $X$ -factor’, which is the ratio of the  $\text{H}_2$  column density to the integrated  $^{12}\text{CO}(1-0)$  line intensity. We use 3D-PDR to post-process hydrodynamic simulations of turbulent, star-forming clouds. We compare the emission of CI and CO for model clouds irradiated by 1 and 10 times the average background and demonstrate that CI is a comparable or superior tracer of the molecular gas distribution for column densities up to  $6 \times 10^{23} \text{ cm}^{-2}$ . Our results hold for both reduced and full chemical networks. For our fiducial Galactic cloud, we derive an average  $X_{\text{CO}}$  of  $3.0 \times 10^{20} \text{ cm}^{-2} \text{ K}^{-1} \text{ km}^{-1} \text{ s}$  and  $X_{\text{CI}}$  of  $1.1 \times 10^{21} \text{ cm}^{-2} \text{ K}^{-1} \text{ km}^{-1} \text{ s}$ .

**Key words:** astrochemistry – hydrodynamics – molecular processes – turbulence – stars: formation – ISM: molecules – photodissociation region (PDR).

# Abstract

- 星形成を探る上で molecular gas の観測は非常に重要
- “CO is uniformly adopted by the star formation community to probe molecular gas” -- however  $X_{\text{CO}}$  has large uncertainty
- 流体シミュレーションで  $X_{\text{CO}}$  と  $X_{\text{Cl}}$  を調べてみる

# Numerical methods

- ORION AMR code (Offner+ 2013)
  - 600 Msun,  $N_{\text{HI}} \sim 5 \times 10^{21}$  の分子雲を作る (typical MW cloud)
  - ガス密度と速度場を計算
- 3D-PDR (Bisbas+ 2012)
  - post-process で温度分布, chemical network を計算
- RADMC-3D
  - non-LTE LVG
  - 密度, アバundance, 温度分布から, 各領域での CO 及び CI flux を計算

# Results

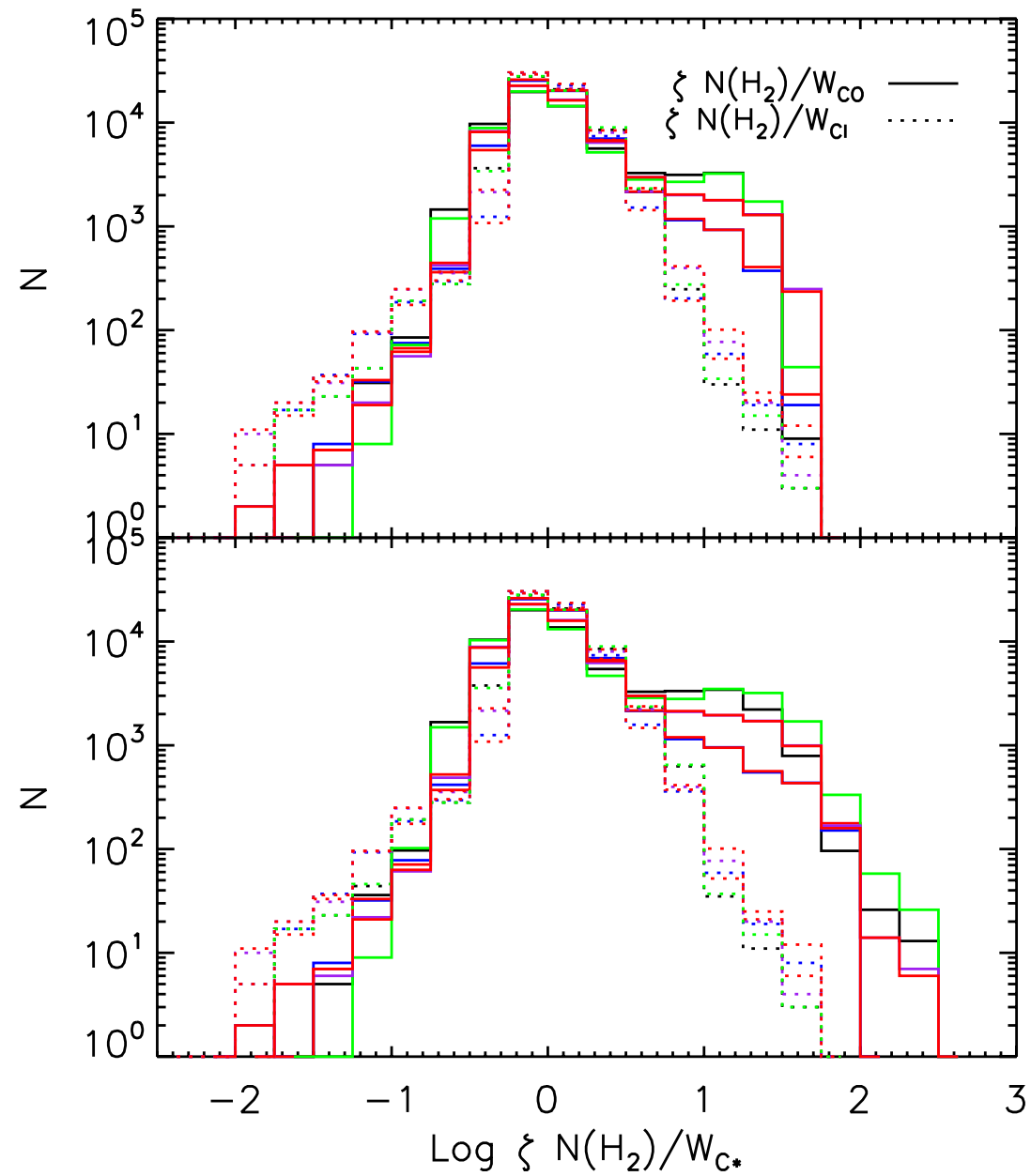


**Figure 1.** Distribution of CO (solid) and C I (dotted) X-factors for six orthogonal views for Rm6\_1.0\_12\_1a. The distributions are normalized to their median value. The bottom panel includes all emission; the top only includes channels with  $T > 0.1$  K.

X factor は非一様

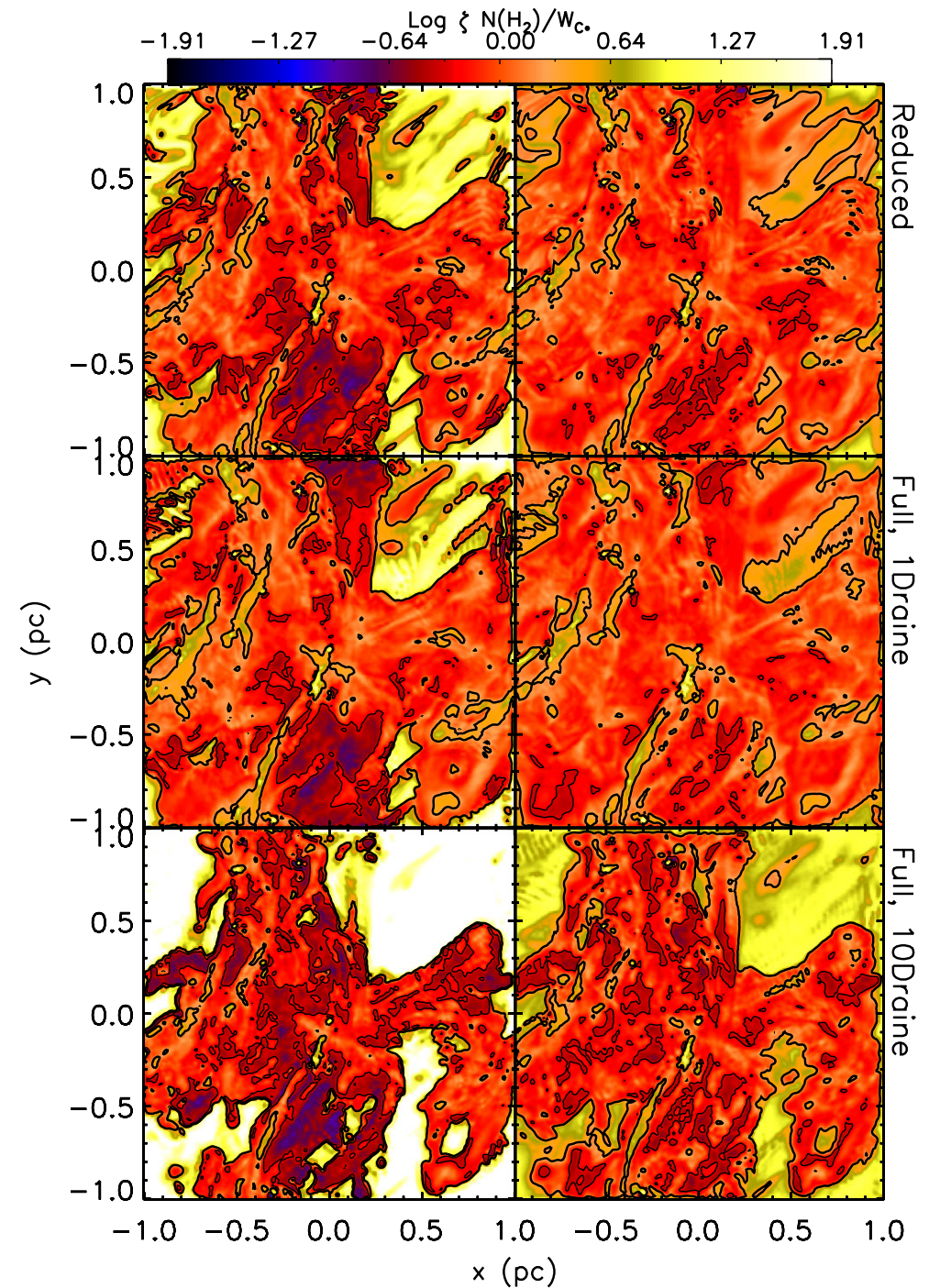


**Figure 2.** Distribution of  $\log \zeta X_{\text{CO}}$  (left) and  $\log \zeta X_{\text{CI}}$  (right) for one view through the simulation for run Rm6\_1.0\_12\_1a (top), Rm6\_1.0\_12\_1f (middle), and Rm6\_1.0\_12\_10f (bottom). The X-factors are normalized to their median value,  $1/\zeta$ . Contours show a factor of 2 above (thick) and below (thin) the median.

# Results

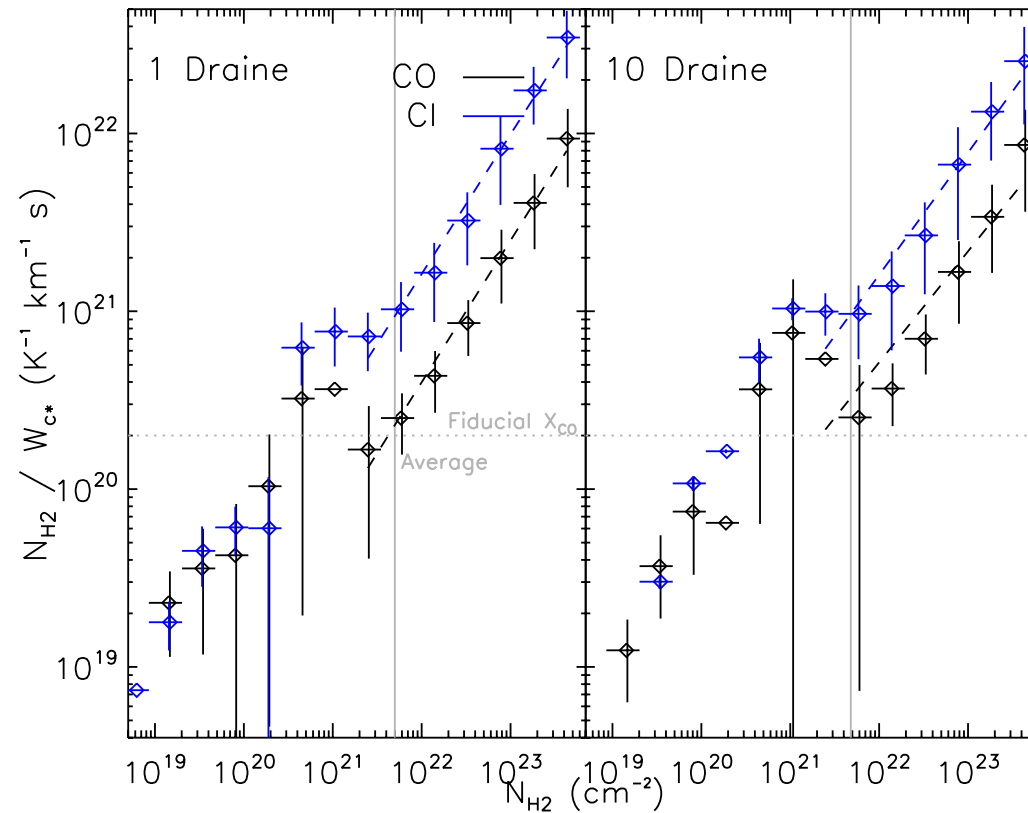


**Figure 3.** CI (blue) and CO (black) mean  $X$ -factors as a function of  $H_2$  column density for one view of Rm6\_1.0\_12\_1f (left) and Rm6\_1.0\_12\_10f (right). The means are obtained from the Fig. 2 data by binning the pixels as a function of their column density. The vertical error bars indicate the standard deviation and the horizontal error bars indicate the bin size. The grey lines show the fiducial CO  $X$ -factor (horizontal dotted) and the mean column density (vertical solid). The dashed lines are least-squares best fits to the data. An online-only figure (Fig. A1) shows the mean  $W_{C^*}$  as a function of  $N_{H_2}$ .

- $X$  factor は  $N_{H_2}$  とよく相関
- $X$  factor が一定と見なせる領域もある
- 密度が低い領域では CI は CO と comparable
- CI のほうが  $X$  factor の分散が小さい (?)

# 結局 PDR 仮定はどこが間違っていたのか？

- 分子雲の非一様性
  - 非一様なら UV photon が染み込みやすくなり, PDR の edge が沢山出来る
  - 実際, シミュレーションの結果では ~73% の mass が 0.01 -- 1.0  $G_0$  の radiation を感じている
- 今回のシミュレーションに入っていないが CI の relative abundance を上げそうな機構
  - Cosmic-ray や UV from massive star による CO の破壊
  - 乱流による mixing
  - 非平衡化学

# Using [CI] to probe the Interstellar Medium in $z \sim 2.5$ Sub-Millimeter Galaxies <sup>\*</sup>

S. Alaghband-Zadeh,<sup>1</sup> S. C. Chapman,<sup>1,2</sup> A. M. Swinbank,<sup>3</sup> Ian Smail,<sup>3</sup> A. L. R. Danielson,<sup>4</sup> R. Decarli,<sup>5</sup> R. J. Ivison,<sup>6,7</sup> R. Meijerink,<sup>8</sup> A. Weiss,<sup>9</sup> Paul. P. van der Werf<sup>10</sup>

## ABSTRACT

We present new [CI](1–0) and <sup>12</sup>CO(4–3) Plateau de Bure Interferometer (PdBI) observations of five Sub-Millimeter Galaxies (SMGs) and combine these with all available [CI](1–0) literature detections in SMGs to probe the gas distribution within a sample of 14 systems. We explore the [CI](1–0) properties of the SMG population, particularly investigating the ratio of the [CI](1–0) luminosity to various <sup>12</sup>CO transition and far-infrared luminosities. We find that the SMGs with new observations extend the spread of  $L_{\text{[CI]}(1-0)}/L_{\text{FIR}}$  to much higher values than found before, with our complete sample providing a good representation of the diverse  $z > 2$  SMG population. We compare the line ratios to the outputs of photodissociation region (PDR) models to constrain the physical conditions in the interstellar medium (ISM) of the SMGs, finding an average density of  $\langle \log(n/\text{cm}^{-3}) \rangle = 4.3 \pm 0.2$  and an average radiation field (in terms of the local field value,  $G_0$ ) of  $\langle \log(G_0) \rangle = 3.9 \pm 0.4$ . Overall, we find the SMGs are most comparable to local ULIRGs in  $G_0$  and  $n$ , however a significant tail of 5 of the 14 SMGs are likely best compared to less compact, local starburst galaxies, providing new evidence that many SMGs have extended star formation distributions and are therefore not simply scaled up versions of local ULIRGs. We derive the ISM properties of a sample of quasars also finding that they have higher densities and radiation fields on average than the SMGs, consistent with the more extreme local ULIRGs, and reinforcing their interpretation as transition objects. We explore the limitations of using simple PDR models to understand [CI], which may be concomitant with the bulk H<sub>2</sub> mass rather than PDR-distributed. We therefore also assess [CI] as a tracer of H<sub>2</sub>, finding that for our sample SMGs, the H<sub>2</sub> masses derived from [CI] are often consistent with those determined from low excitation <sup>12</sup>CO. We conclude that [CI] observations provide a useful tool to probe the bulk gas and gas processes occurring within merging SMGs, however more detailed, resolved observations are required to fully exploit [CI] as a diagnostic.

# Abstract

- high-z では high-J CO は観測されているが,そこで観ているのは warm dense gas である
- CI のほうが high-J CO よりは H<sub>2</sub> 全体をよくトレースするかもしれない
- local ULIRG では CI が H<sub>2</sub> をトレースするのは実証済み
- high-z SMG では Walter et al. (2011) がこれまでで最大のサンプル数
- high-z SMGs でも [CI]/CO や [CI]/FIR は MW と変わらない?
- しかし Walter sample はほとんど全てレンズされているため不定性がある

# Sample selection & Observation

- 5 個の un-lensed SMGs at  $z \sim 2.3$  を select
- H $\alpha$  が受かっている、ALMA から見えるもの
- CI(1-0), I2CO(4-3) を IRAM PdBI で観測

ID	RA	Dec	$z$	$t_{\text{CO}(4-3)}$ (hrs)	$t_{\text{[CI]}(1-0)}$ (hrs)	$S_{2\text{mm}}$ (mJy)	$S_{850\mu\text{m}}$ (mJy)	$\nu_{\text{obs,CO}(4-3)}$ GHz	$\nu_{\text{obs,[CI]}(1-0)}$ GHz
<i>SXDF7 (J0217-0505)</i>	02:17:38.92	-05:05:23.7	2.5286[8]	3.2	5.1	$0.3 \pm 0.1$	$7.1 \pm 1.5$	130.6	139.4
<i>SXDF11 (J0217-0459)</i>	02:17:25.12	-04:59:37.4	2.2821[8]	3.3	3.3	-	$4.5 \pm 1.9$	138.5	148.9
<i>SXDF4a (J0217-0503a)</i>	02:17:38.62	-05:03:37.5	2.0298[2]	2.1	7.8	$0.5 \pm 0.1$	$2.2 \pm 0.85$	151.9	162.2
<i>SXDF4b (J0217-0503b)</i>	02:17:38.62	-05:03:37.5	2.0274[1]	2.1	7.8	$0.4 \pm 0.1$	$2.2 \pm 0.85$	151.9	162.2
<i>SA22.96 (J2218-0021)</i>	22:18:04.42	00:21:54.4	2.5169[7]	3.0	5.3	$0.2 \pm 0.1$	$9.0 \pm 2.3$	131.1	139.9

**Table 1.** SMG positions from the 1.4 GHz detections, and redshifts from the second order moment analysis of the  $^{12}\text{CO}(4-3)$  observations of this work. The IDs in italics indicate the IDs used for the H $\alpha$  observations in Alaghband-Zadeh et al. (2012). The 2 mm continuum is measured in the off-line regions of the [CI](1-0) observations, which are deeper and also at slightly higher frequency than the  $^{12}\text{CO}(4-3)$  observations. The 850  $\mu\text{m}$  fluxes are from Chapman et al. (2005) and Coppin et al. (2006). The values in brackets in the redshift column represent the error on the last decimal place. Since we detect approximately equal 2 mm continuum across both SXDF4a and SXDF4b, the  $S_{850\mu\text{m}}$  values for SXDF4a and SXDF4b assume the measured 850  $\mu\text{m}$  flux for the whole system is equally divided between the two components. We also quote the 5 antennae on-source times ( $t$ ) and the observing frequencies ( $\nu$ ).

ID	Beam Size $_{\text{[CI]}(1-0)}$	Physical Scale $_{\text{[CI]}(1-0)}$	Beam Size $_{\text{CO}(4-3)}$	Physical Scale $_{\text{CO}(4-3)}$
	(arcsec)	(kpc)	(arcsec)	(kpc)
<i>SXDF7</i>	$4.4 \times 3.5$	$40 \times 30$	$7.1 \times 3.6$	$60 \times 30$
<i>SXDF11</i>	$8.0 \times 3.2$	$70 \times 30$	$4.4 \times 3.5$	$40 \times 30$
<i>SXDF4</i>	$5.1 \times 2.7$	$40 \times 20$	$4.4 \times 3.3$	$40 \times 30$
<i>SA22.96</i>	$4.8 \times 3.2$	$40 \times 30$	$4.5 \times 3.8$	$40 \times 30$

**Table 2.** The beam sizes of the [CI](1-0) and  $^{12}\text{CO}(4-3)$  observations and the approximate physical scales (in kpc) corresponding to these beam sizes.

# S/N map of SXDF7

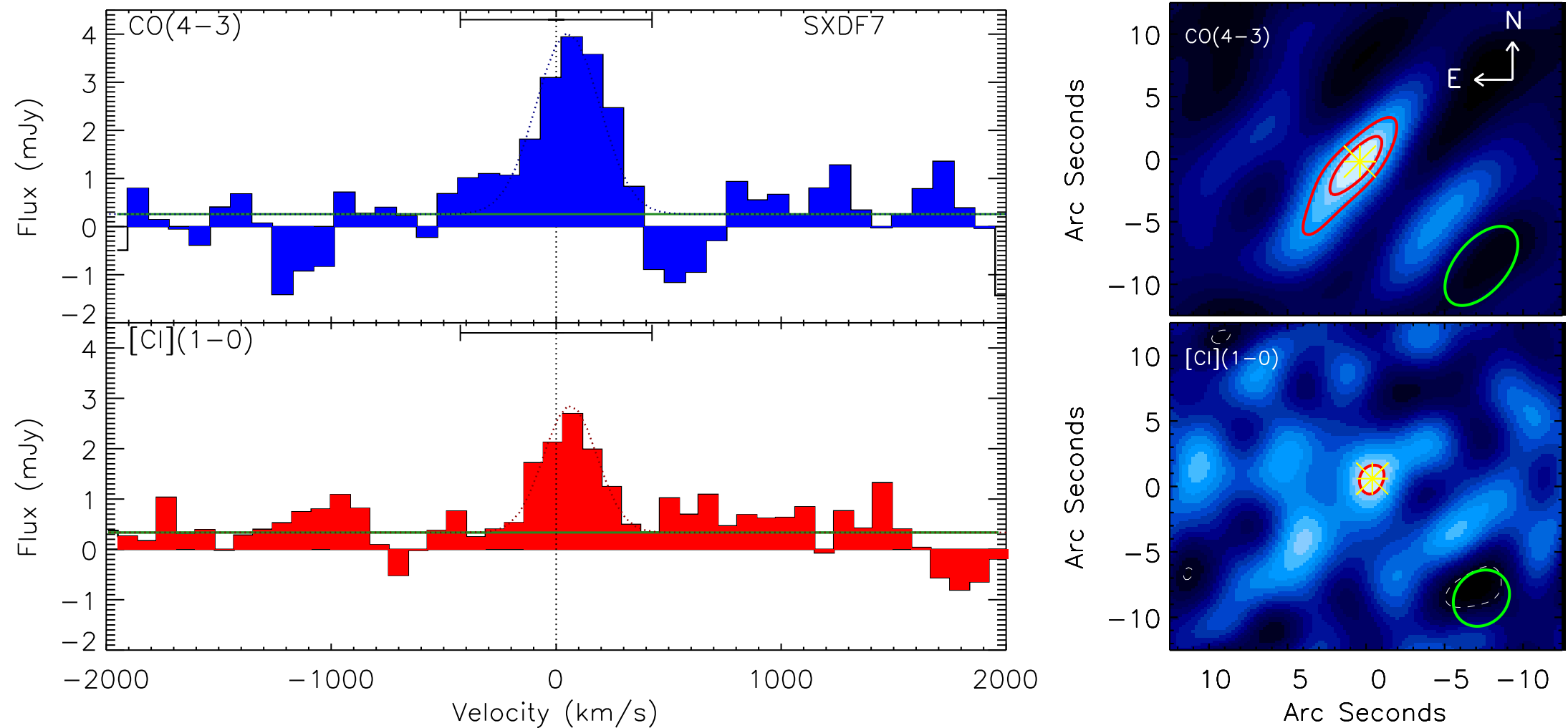


**Figure 1.** SXDF7: Top:  $^{12}\text{CO}(4-3)$  spectrum (left) extracted from the peak pixel of the velocity-integrated S/N map (right) marked by a star. The contours of the S/N map represent the S/N starting at the  $\pm 3\sigma$  level (solid red for positive  $\sigma$  levels and dashed white for negative  $\sigma$  levels). The noise is derived from the standard deviation of the flux outside the velocity channels over which the spectra were integrated to measure the intensities. Bottom:  $[\text{CI}](1-0)$  spectrum (left) extracted the pixel marked in the velocity-integrated S/N map (right). The region marked over the spectra represent the velocity channels over which the spectra were integrated to gain the total line fluxes, as determined from the second order moment analysis of the  $^{12}\text{CO}(4-3)$  spectrum ( $\pm 2\sigma$ ). The spectra are centred such that the zero velocity corresponds to the redshift of the  $^{12}\text{CO}(4-3)$  detection. The solid horizontal green lines in the spectra represent the continuum level which was subtracted prior to the moment analysis. The green ellipses on the bottom right of the S/N maps represent the beam sizes and shapes. The maps are centred at RA=02:17:38.885 and Dec=-05:05:27.971.

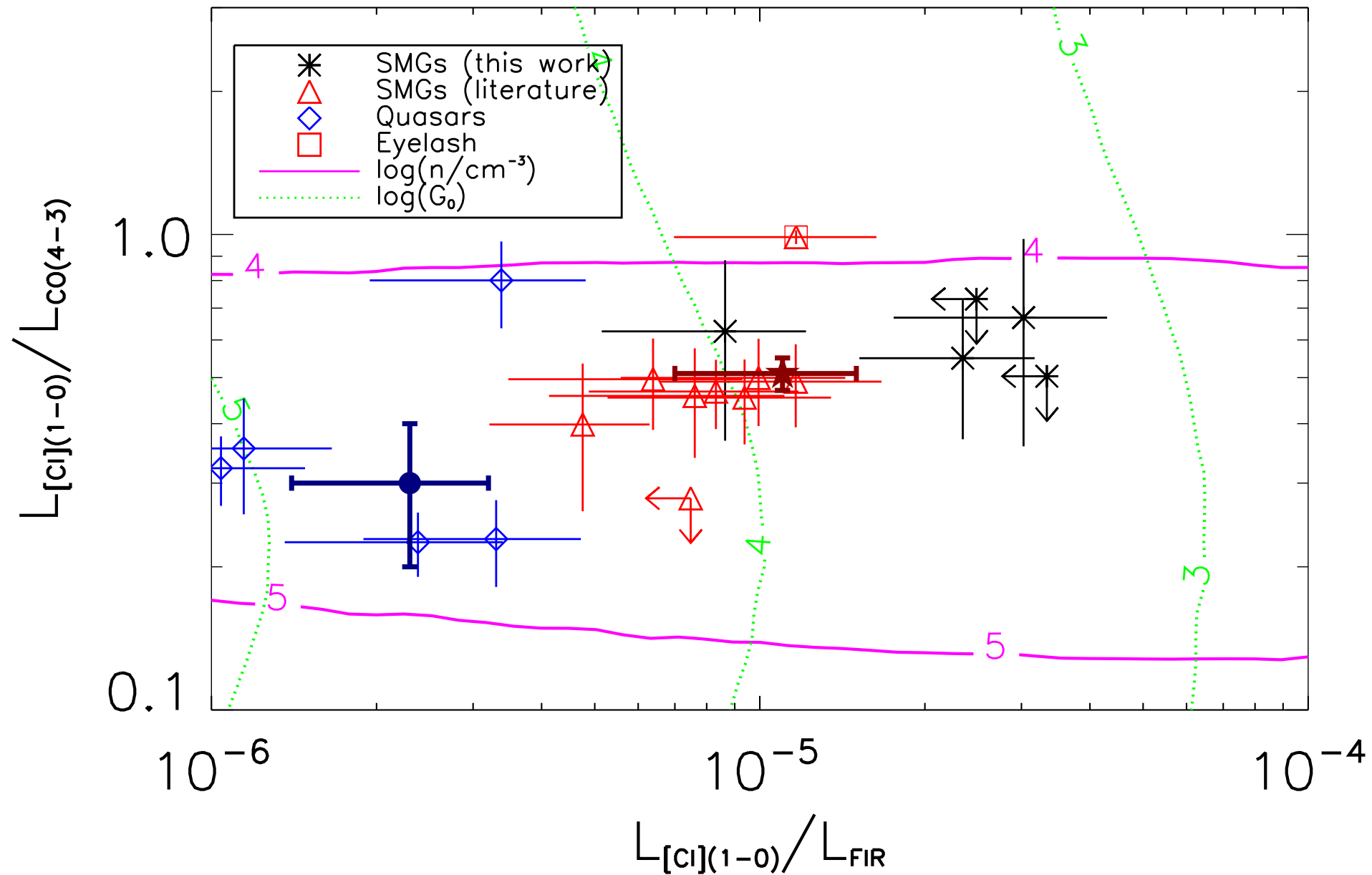
空間分解出来た天体は無し

# 観測結果 まとめ

ID	$L'_{[\text{CI}](1-0)}$ ( $10^{10}\text{K kms}^{-1}\text{ pc}^2$ )	$L'_{[\text{CI}](2-1)}$ ( $10^{10}\text{K kms}^{-1}\text{ pc}^2$ )	$L'_{\text{CO}(4-3)}$ ( $10^{10}\text{K kms}^{-1}\text{ pc}^2$ )	$L'_{\text{CO}(3-2)}$ ( $10^{10}\text{K kms}^{-1}\text{ pc}^2$ )	$L'_{\text{CO}(1-0)}$ ( $10^{10}\text{K kms}^{-1}\text{ pc}^2$ )	$L_{\text{FIR}}$ ( $10^{13}L_{\odot}$ )	$\mu$
SXDF7	$1.3\pm 0.3$	-	$2.9\pm 0.6$	$3.7\pm 0.8$	$7\pm 2$	$0.21\pm 0.05$	1
SXDF11	$< 1.0$	-	$1.6\pm 0.3$	$2.0\pm 0.4$	$3.9\pm 0.8$	$0.15\pm 0.05$	1
SXDF4a	$0.7\pm 0.3$	-	$1.4\pm 0.4$	$1.7\pm 0.5$	$3\pm 1$	$0.09\pm 0.02$	1
SXDF4b	$< 0.8$	-	$2.0\pm 0.6$	$2.5\pm 0.8$	$5\pm 2$	$0.09\pm 0.02$	1
SA22.96	$1.2\pm 0.4$	-	$2.3\pm 0.6$	$6\pm 2$	$6\pm 2$	$0.5\pm 0.1$	1
J02399	$1.5\pm 0.2$	$0.5\pm 0.3$	$3.8\pm 0.5$	$4.9\pm 0.6$	$8\pm 2$ ( $9\pm 1$ )	$0.7\pm 0.3$	2.5
J123549	$1.4\pm 0.3$	$< 0.5$	$3.4\pm 0.3$	$4.4\pm 0.4$	$7.5\pm 0.9$ ( $8.4\pm 0.8$ )	$0.5\pm 0.2$	1
J163650	$< 1$	$< 1$	$4.6\pm 0.3$	$5.9\pm 0.4$	$9\pm 1$ ( $11.3\pm 0.8$ )	$0.5\pm 0.2$	1
J163658	$1.4\pm 0.3$	$< 1$	$3.7\pm 0.5$	$4.7\pm 0.6$	$10\pm 2$ ( $9\pm 1$ )	$0.7\pm 0.3$	1
J14011	$0.7\pm 0.$	$0.48\pm 0.05$	$1.9\pm 0.2$	$2.4\pm 0.3$	$2.4\pm 0.2$ $4.5\pm 0.5$	$0.2\pm 0.1$	4
J16359	$0.12\pm 0.02$	$0.043\pm 0.008$	$0.33\pm 0.03$	$0.42\pm 0.03$	$0.80\pm 0.08$	$0.05\pm 0.02$	22
J213511	$0.69\pm 0.02$	$0.26\pm 0.01$	$0.85\pm 0.01$	$1.159\pm 0.009$	$1.71\pm 0.09$ ( $2.08\pm 0.02$ )	$0.23\pm 0.09$	32.5
ID141	$0.5\pm 0.2$	$0.24\pm 0.08$	$1.6\pm 0.2$	$2.1\pm 0.2$	$3.9\pm 0.5$	$0.43\pm 0.02$	20
MM18423+5938	$0.39\pm 0.08$	$0.26\pm 0.05$	$0.95\pm 0.01$	$1.20\pm 0.01$	$2.31\pm 0.02$	$0.23\pm 0.09$	20

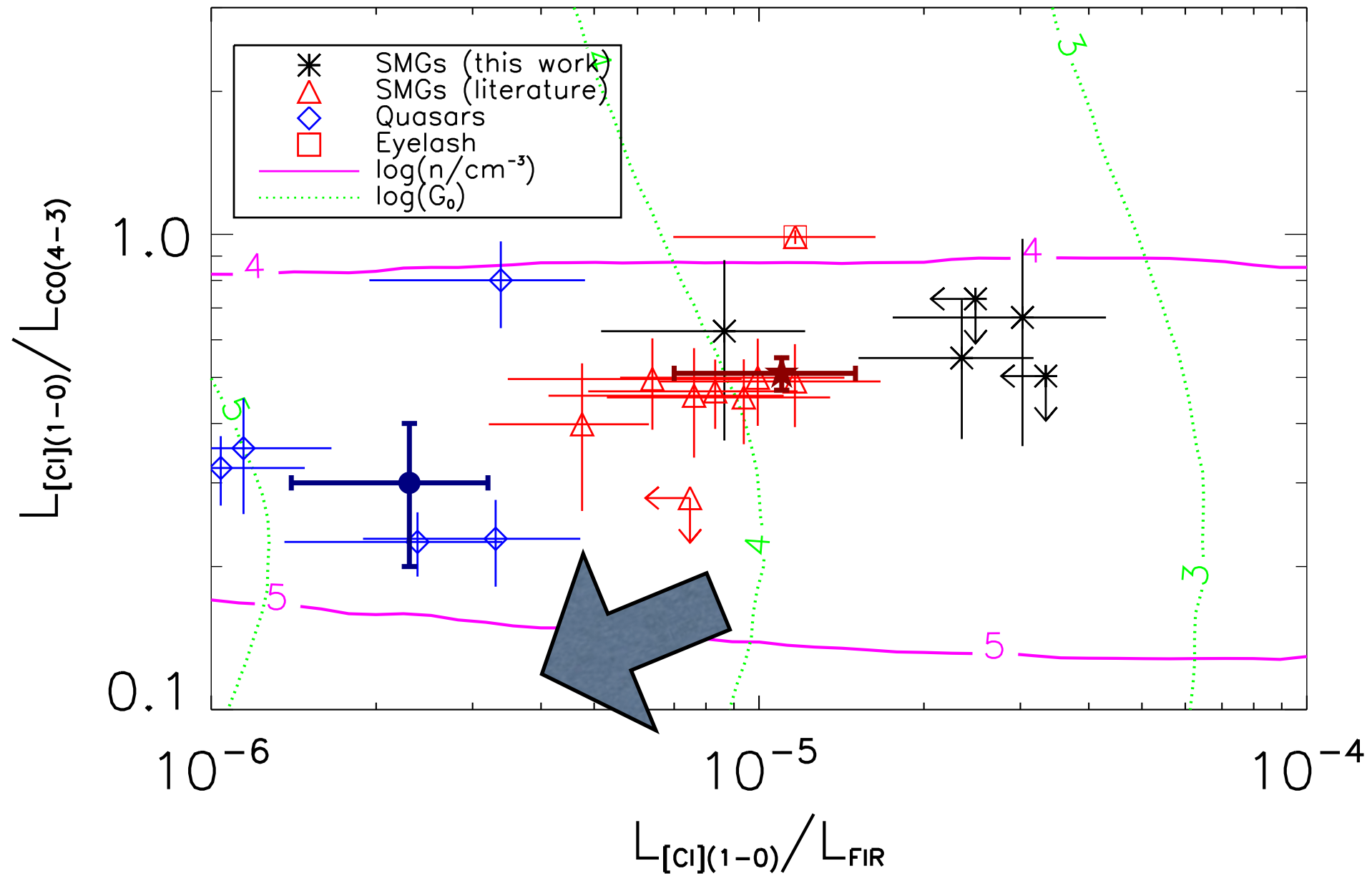
**Table 5.** Line luminosities and quoted magnification factors for the SMGs studied in this work (top) and the literature SMG sample (bottom). Where certain  $^{12}\text{CO}$  transition line luminosities are not directly measured the values quoted are inferred from other  $^{12}\text{CO}$  transitions using the conversions from Bothwell et al. (2013) and are shown in italics. All luminosities are corrected for gravitational lensing using the magnification factors in column ( $\mu$ ). The far-infrared luminosities are derived from integrating under a modified blackbody curve from 8-1000  $\mu\text{m}$ . The magnification value we use for J14011 is 4 since the range of possible magnifications is 3–5 (Smail et al. 2005). The magnification value we use for ID141 is 20 since the range of possible magnifications is 10–30 (Cox et al. 2011). Since we detect approximately equal continuum across both SXDF4a and SXDF4b, the  $L_{\text{FIR}}$  values for SXDF4a and SXDF4b assume that the observed  $L_{\text{FIR}}$  is divided equally between the two components of this system.

# luminosity ratios of SMGs



- 高い  $L_{CI} / L_{FIR}$  を持つ SMGs を新たに発見
- SFR の割に gas mass が大きいような銀河？

# luminosity ratios of SMGs



• non-PDR なら左下に動く

# PDR analysis

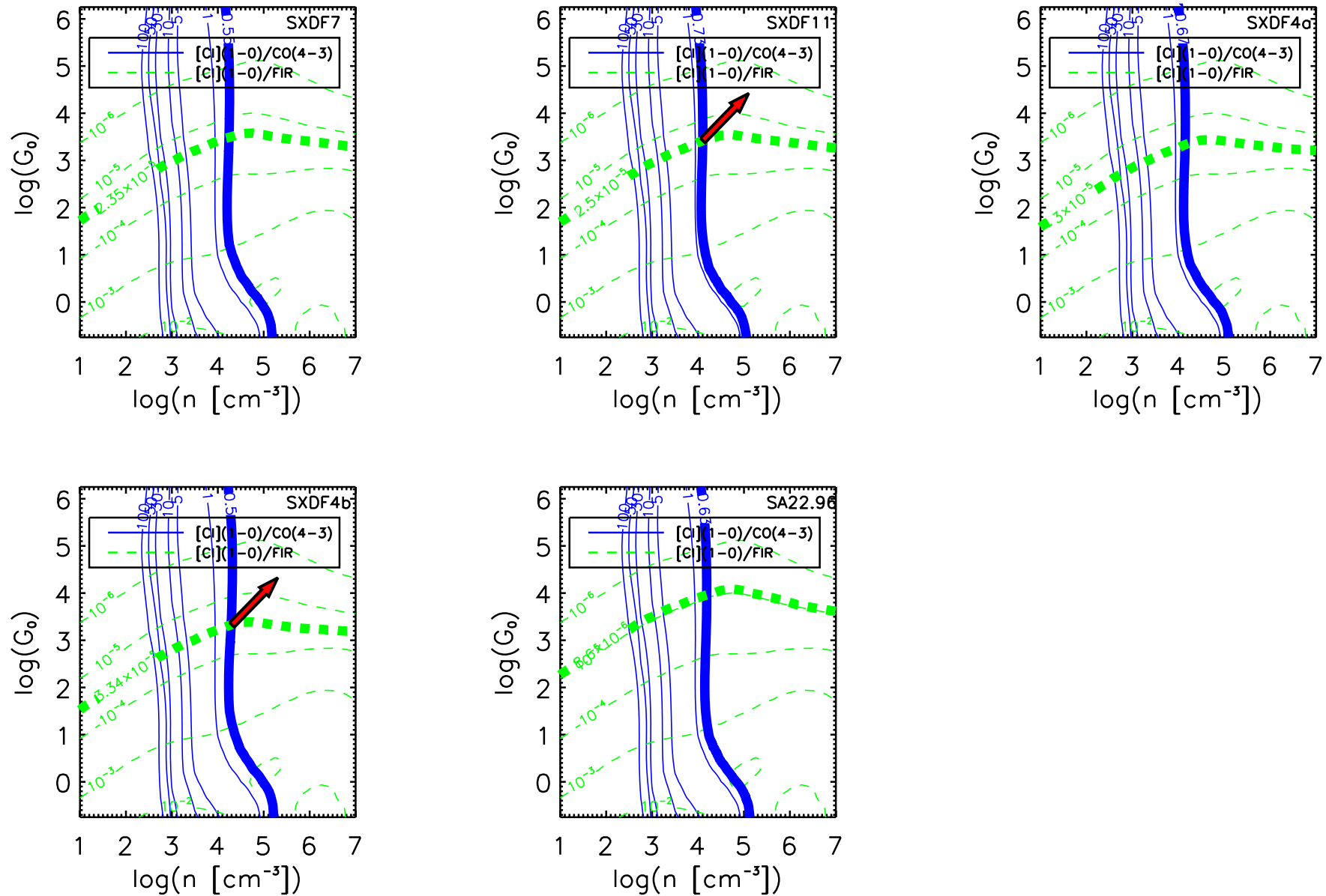


**Figure A1.** Contours of  $L_{[\text{C I}](1-0)}/L_{\text{CO}(4-3)}$  (solid blue) and  $L_{[\text{C I}](1-0)}/L_{\text{FIR}}$  (dashed green) at various levels of gas density ( $n$ ) and radiation field ( $G_0$ ) from the PDR models of Kaufman et al. (1999). The bold contours represent the observed ratios for each of the SMGs with new [C I] detections presented in this work. The intersection of the two contours in each case provides a value for  $n$  and  $G_0$  for the SMG system. The red arrows mark the sources where there is only a limit to the [C I](1–0) luminosity and therefore we can only gain a lower limit to  $n$  and  $G_0$ .

# PDR analysis

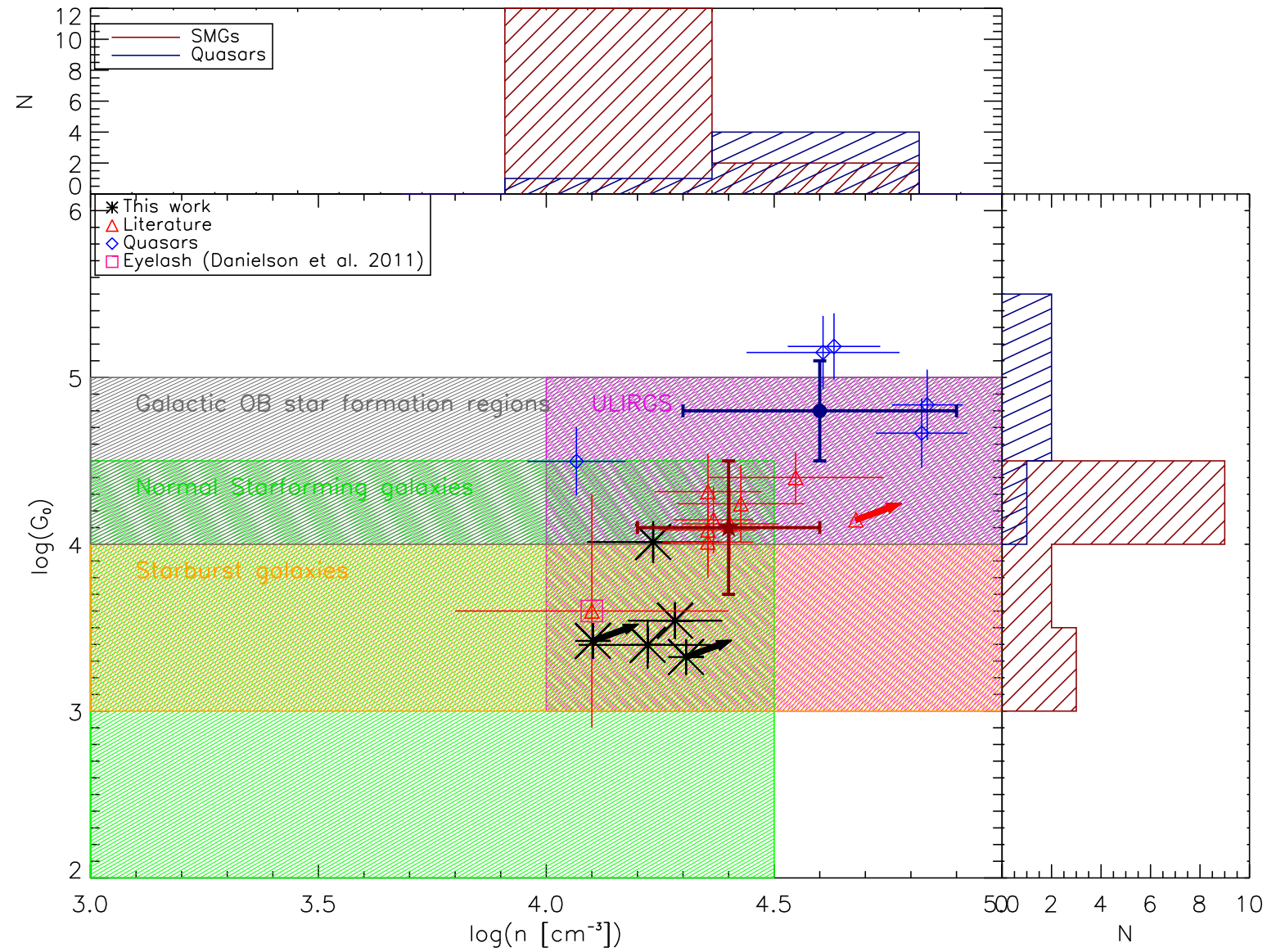


**Figure 9.** The far-UV radiation field, in terms of the local value ( $G_0$ ), against the gas density ( $n$ ) derived from the comparison of various [C I],  $^{12}\text{CO}$  and far-infrared luminosities to the outputs from the Kaufman et al. (1999) PDR models. We plot the derived values for the SMGs and the literature quasars. The median values for the complete SMG and quasar samples are marked by the dark red filled star and dark blue filled circle respectively. We also mark the ranges in  $n$  and  $G_0$  derived for other populations - local ULIRGs, Galactic OB star-formation regions, normal star-forming galaxies and starburst galaxies (Stacey et al. 1991; Malhotra et al. 2001; Davies et al. 2003). We find that the SMGs are most comparable to the local ULIRGs although the tail of 5 SMGs with lower densities and radiation field values are more consistent with local starburst galaxies.

local ULIRG っぽい SMGs と、  
もう少し大人しい SMGs が居る

# Gas mass

- 励起温度  $T_{\text{ex}} \sim 30\text{K}$  を仮定して  
carbon mass を導出
- $X[\text{CI}]/X[\text{H}_2] \sim 5 \times 10^{-5}$  (local value) を  
仮定して CI mass から  $\text{H}_2$  を導出
- $^{12}\text{CO}(1-0)$  から求めた  $\text{H}_2$  mass と  
コンパラ  $\Rightarrow$  CI は  $\text{H}_2$  mass の指標  
として使える
- ALMA なら  $\text{CI}(2-1)$  と  $\text{CI}(1-0)$  を同  
時に検出して  $T_{\text{ex}}$  を求められる

ID	$M_{[\text{CI}]}$ $10^7 M_{\odot}$	$M_{[\text{CI}](\text{H}_2)}$ $10^9 M_{\odot}$	$M_{\text{CO}(\text{H}_2)}$ $10^9 M_{\odot}$
SXDF7	$1.6 \pm 0.4$	$120 \pm 30$	$70 \pm 20$
SXDF11	$< 1.2$	$< 90$	$39 \pm 8$
SXDF4a	$0.9 \pm 0.3$	$70 \pm 20$	$30 \pm 10$
SXDF4b	$< 1.0$	$< 70$	$50 \pm 20$
SA22.96	$1.5 \pm 0.5$	$110 \pm 30$	$60 \pm 20$
J02399	$1.8 \pm 0.2$	$130 \pm 20$	$80 \pm 20$
J123549	$1.8 \pm 0.3$	$130 \pm 20$	$74 \pm 9$
J163650	$< 1.3$	$< 90$	$90 \pm 10$
J163658	$1.7 \pm 0.4$	$120 \pm 30$	$100 \pm 20$
J14011	$0.9 \pm 0.2$	$70 \pm 10$	$24 \pm 3$
J16359	$0.16 \pm 0.03$	$11 \pm 2$	$8.2 \pm 0.8$
J213511	$0.87 \pm 0.03$	$61 \pm 3$	$17.1 \pm 0.9$
ID141	$0.7 \pm 0.2$	$50 \pm 20$	$39 \pm 5$
MM18423+5938	$0.5 \pm 0.1$	$34 \pm 8$	$23.1 \pm 0.2$

**Table 7.** The neutral carbon masses and molecular gas masses calculated from the  $^{12}\text{CO}(1-0)$  and  $[\text{CI}](1-0)$  luminosities for the SMGs with new  $[\text{CI}](1-0)$  observations in this work and the literature sample of SMGs.

# まとめ

- CI(1-0) と  $12\text{CO}(4-3)$  の観測を合わせて SMGs の ISM の物理状態を探った
- SMGs には local ULIRG 的なものも, normal star forming 的なものも居る
- CI と CO を合わせることで PDR model から  $G_0$  と  $n$  を一意に決められる
- CI は  $\text{H}_2$  mass のトレーサーとして使える
- ただし, PDR model が本当に正しいのかは要検証

# 全体のまとめ

- [CI]を観ることで, ISM の物理状態により強い制限が付けられる
- [CI]は H<sub>2</sub> mass tracer となりうるが, PDR に代わるモデルを空間分解した観測で検証する必要あり
- CO よりも [CI] の方が明るい場合も？
- SMGs も一枚岩ではない
- CI と high-J CO では違うガスを観ている？
- 星形成に関わるガスと関わらないガスを切り分けられれば星形成モデルに制限がつくかも